ExpeER
Distributed Infrastructure for EXPErimentation in Ecosystem Research

Grant Agreement Number: 262060

SEVENTH FRAMEWORK PROGRAMME

CAPACITIES
INTEGRATING ACTIVITIES: NETWORKS OF RESEARCH INFRASTRUCTURES (RIS)
THEME: ENVIRONMENT AND EARTH SCIENCES

DELIVERABLE D7.4

Deliverable title: Evaluation report on the use of multiple technologies to observe soil moisture and water fluxes

Abstract: This report summarizes the results of a combined field site test of wireless soil moisture sensing and mobile electromagnetic induction measurements to describe states and transition dynamics of soil moisture at the field scale

Due date of deliverable: M36 Actual submission date: M50

Start date of the project: December 1st, 2010 Duration: 54 months

Organisation name of lead contractor: UFZ

Contributors: Edoardo Martini, Ute Wollschläger, Ulrike Werban, Steffen Zacharias

Revision N°: FINAL

Dissemination level:

PU Public (must be available on the website)	**X**
PP Restricted to other programme participants (including the Commission Services)	**[ ]**
RE Restricted to a group specified by the consortium (including the Commission Services) (precise to whom it should be addressed)	**[ ]**
CO Confidential, only for members of the consortium (including the Commission Services)	**[ ]**

Table of Content

1. EXECUTIVE SUMMARY 1

2. INTRODUCTION 1

3. SITE DESCRIPTION 2

4. METHODS 3

4.1. SITE EXPLORATION 3

4.2. SELECTION OF SOIL MOISTURE MONITORING LOCATIONS 4

4.3. PEDOLOGICAL CHARACTERIZATION 5

4.4. SOIL MOISTURE MEASUREMENTS 7

4.5. ELECTROMAGNETIC INDUCTION (EMI) MEASUREMENTS 9

4.6. ECA DATA PROCESSING 9

4.7. STATISTICAL ANALYSIS OF THE CHARACTERISTIC STATES OF SOIL MOISTURE (MARTINI ET AL, SUBMITTED) .. 10

5. RESULTS 12

5.1. DESCRIPTION OF CHARACTERISTIC STATES OF SOIL MOISTURE USING A WIRELESS SOIL MOISTURE SENSING NETWORK 12

5.2. SUITABILITY OF REPEATED EMI SURVEYS TO MAP SPATIAL PATTERNS OF SOIL MOISTURE DYNAMICS 14

6. DISCUSSION AND CONCLUSION 17

7. REFERENCES 19

1. Executive summary

This report summarizes results of Task 7.3 “New sensor technologies for integrated observation of soil moisture at the field scale and landscape scale. The study aimed to explore new and innovative sensors, novel measurement technologies and its combination for an improved assessment of soil moisture. Fort this report, results of a field test of a wireless soil moisture sensing network (WSN) and mobile applications of electromagnetic induction (EMI) measurements are presented.

It could be shown, that WSNs are an excellent tool to describe persistence and transition mechanisms of soil moisture states and patterns. An innovative method of data analysis using the Spearman rank correlation coefficient is proposed. It allows detailed qualitative assessment of spatial and temporal soil moisture patterns.

Mobile electromagnetic induction surveys are an excellent tool to map soil spatial distribution at the field scale. Nevertheless, the suitability of EMI to characterize soil moisture dynamics at the specific study site was poor. Consequently, the sound interpretation of EMI signals with respect to soil moisture requires profound understanding of underlying hydrological processes and pedological expertise.

2. Introduction

Soil moisture is a key state variable for the terrestrial environment, determines both the storage and the generation of runoff processes, and controls the exchange of water and energy in the land-atmosphere system. By this, soil moisture is a critical state variable for every hydrological or meteorological model. While there is no doubt about the critical role of soil moisture, it is still a great challenge to provide adequate information about soil moisture distribution beyond the point scale (Brocca et al., 2010; Grayson and Blöschl, 2001; Mohanty and Skaggs, 2001; Romano, 2014; Vanderlinden et al., 2012; Vereecken et al., 2014). Soil moisture is highly variable both in time and space, thereby considerably hampering the estimation of soil moisture at larger scales.

Wireless sensor networks (WSNs) are an emerging technology in soil monitoring and its application in environmental monitoring is increasingly spreading (Bogena et al., 2007; Hansen, 2005; Moghaddam et al., 2010; Ritsema et al., 2009; Robinson et al., 2008; Savva et al., 2013; Terzis et al., 2010). Wireless sensor networks allow a near real-time monitoring of soil moisture variability. With the growing availability of low-cost soil moisture sensors, WSNs are a promising tool to bridge the scale gap between point measurements of soil moisture and the understanding of hydrological behavior at the field scale. By this, WSN offer the opportunity to observe soil water processes at scale relevant for watershed management and to bridge point-based measurements and remote sensing.

Among proximal soil sensing, measuring the soil apparent electrical conductivity (ECa) using electromagnetic induction (EMI) is widely used (Corwin and Lesch, 2005; Kachanoski et al., 1988; Robinson et al., 2008; Scull et al., 2003; Werban et al., 2013; Zhu et al., 2010). EMI allows a fast and relatively cost-effective exploration of large areas. EMI allows fast and relatively low-cost mapping of large volumes of soil apparent electrical conductivity (ECa), which is influenced by several factors (McNeil, 1980) including clay content (e.g., Doolittle et

al., 2002), gravel content (e.g., Priori et al., 2010), soil moisture (e.g., Huth and Poulton, 2007; Cousin et al., 2009; Zhu et al., 2010; Robinson et al., 2012), salinity (e.g., Triantafilis et al., 2000), soil compaction (e.g., André et al., 2012), and clay-pan depth (e.g., Sudduth et al., 2005), among others. Traditional soil sampling and EMI techniques can be used together to provide even more comprehensive information on soil spatial variability than is possible using either approach alone (Martini et al., 2013; Priori et al., 2013; Doolittle and Brevik, 2014).

However, since the factors affecting ECa vary, a sound interpretation with respect to soil moisture is a challenge. Repeated EMI surveys have the potential to reveal temporal changes in the factors affecting ECa and may be one way to reconstruct the soil moisture influence in the ECa signal and towards a field-scale exploration of soil moisture dynamics (Zhu et al., 2010; Robinson et al., 2012).

Among proximal soil sensing techniques, gamma-ray spectrometry is a suitable method for mapping physical parameters related to soil properties (Dierke and Werban, 2013). The measured natural gamma radiation in soils depends on soil parameters, which are the result of composition and properties of parent rock and processes during soil genesis under different climatic conditions. Grain size distribution, type of clay minerals and organic matter content are soil properties which influence directly the gamma-ray concentration (Fertl, 1979), and such relations at the field scale are site specific (Dierke and Werban, 2013).

The study aimed to (i) develop an efficient strategy for monitoring soil moisture dynamics at the field scale by combining soil hydrological and pedological expert knowledge with geophysical measurement techniques, (ii) develop a method for data analysis allowing the identification relevant hydrological states and processes based on large data sets, and (iii) test the suitability of EMI for the characterization of soil moisture patterns. The hydrological characterization of the study site refers in large parts the work of Martini et al. (submitted).

3. Site Description

The study site is located within the Schäfertal experimental site. The Schäfertal is a small headwater catchment (1.44 km²) located in the Lower Harz Mountains in Central Germany (51°39’N, 11°03’E). The experimental site was established at the end of the 1960s. At this time a hydro-meteorological station and three transects of groundwater level gauges were put into place (Becker and McDonnell, 1998). Since then the research infrastructure has been continuously expanded and today an extensive time series of meteorological data, discharge records, groundwater level recordings, and numerous additional environmental variables is available. The site is managed and operated by the Magdeburg-Stendal university of Applied Sciences. In 2010, the Schäfertal experimental site was selected to be further expanded to be one of the intensive test sites of the TERENO observatory Harz/Central German Lowland (Zacharias et al., 2011). Since this time, the research infrastructure has been substantially enhanced and now also includes e.g. lysimeters, a wireless soil moisture sensing network, several cosmic ray soil moisture probes, a snow monitoring system, and is one of the central calibration/validation sites for remote sensing campaigns within the TERENO observatory.

The average annual precipitation is only 630 mm (time series 1968-2008).The average annual temperature 6.8 °C. The slightly subcontinental character of the climate is reflected

by a higher probability of early (September) or late (May) frost events. Absolute minimum temperatures can be below -20 °C. Furthermore, there is a high probability for snow during the winter months.

Geologically, the region is formed by greywacke and argillaceous slate which are covered by sediments of periglacial origin (Borchardt, 1982). Along the slopes of the catchment, between an upper permeable soil layer and the bedrock, near-surface compacted horizons exists, which are known to trigger interflow Between the soil surface and the bedrock, whilst part of the interflow can reach the surface again by return flow (Becker and McDonnell, 1998; Borchardt, 1982). Dominant soil types in the Schäfertal are Gleysols occurring in the wet valley bottom as well as Luvisols and Cambisols on the loess-covered slopes (Ollesch, 2008).

For the present study, a smaller hillslope area downstream of the Schäfertal gauging station was selected for a detailed study of unsaturated zone hydrological processes. The site includes a north and a south exposed slope which are divided by the creek (Schäferbach) in the valley bottom (Figure 1). In contrast to the slopes upstream of the gauging station which are primarily covered by cropland, the study site is completely covered with pasture and is not affected by agricultural practices except that the grass is cut once or twice per year. The spatial extent of the hillslope is ca. 250 by 80 m. The site presents varying topographical and pedological features, and, as for the entire catchment, lateral flows are expected to play a relevant role within the runoff generation (Martini et al., submitted).

4. Methods

4.1. Site exploration

The soil spatial variability of the hillslope area was investigated using a combination of geophysical measurements, topographic information, and classical pedological observations. Such information can be used as input covariate for geostatistical sampling strategies in order to select a number of sampling locations which represent the range of variability of the input variables (Minasny and McBratney, 2006). However, only in situ pedological observations can provide direct information on spatial variability of soil characteristics such as soil layering, texture and soil morphology, which are all relevant for understanding hydrological process within the area under investigation. Such time-consuming survey can be optimized with the help of statistical analyses based on high-resolution spatial information gained with geophysical measurements.

Prior to the start of the monitoring period, preliminary measurement campaigns have been carried out at different times, which reflect different moisture and soil temperature states, in order to map the soil spatial variability of the site under investigation. In August 2011, January 2012 and April 2012, soil apparent electrical conductivity (ECa) was measured with two electromagnetic induction (EMI) devices (EM38-DD and EM38-MK2, Geonics Ltd., Ontario, Canada) using a sampling rate of 5 records/s.

An extensive description of the theory of electromagnetic induction and field measurements is provided in a separate section. In August 2011, concentrations of ^{40}K, ^{238}U, ^{232}Th and total counts were measured using a portable gamma-ray spectrometer with a 4-liter thallium-

activated NaI (sodium iodide) crystal (GF Instruments, Czech Republic). A counting period of 5 s was applied.

4.2. Selection of soil moisture monitoring locations

Conditioned Latin hypercube sampling (cLHS) was applied to select a calibration sample set for soil moisture monitoring based on interpolated geophysical measurements within the study area. The method was first introduced by Minasny and McBratney (2006) to ensure a full coverage of the state space of each predictor as well as to preserve the correlation between the predictors in the sample set. For the present work, interpolated and uncorrelated ($r < 0.7$) geophysical data (with spatial resolution of 1 m) were used as predictors.

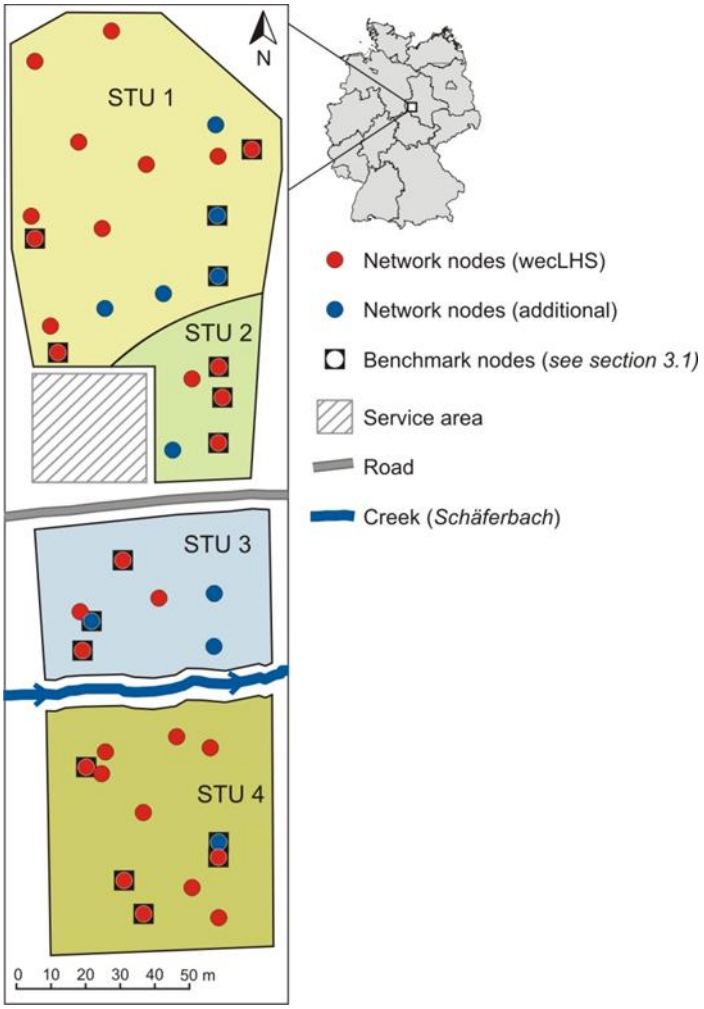

Figure 1 *- The study area and the spatial distribution of the 40 nodes of the soil moisture monitoring network. The four Soil Topographic Units (STUs) were classified according to the pedological description of soil profiles for each of the 40 locations indicated in the map, and mirror very well the spatial pattern obtained with geophysical proximal soil sensing techniques. The benchmark nodes were used for the statistical analysis of soil moisture data.*

For the present work, the geophysical data mentioned in the previous section were used as ancillary information for the weighted conditioned Latin hypercube sampling (wecLHS, described in Schmidt et al., 2014). With such sampling scheme, we aim to represent the variability of both static and dynamic soil characteristics, as observed by the geophysical measurements and being related to soil texture, soil organic matter and soil moisture.

After selecting 30 monitoring locations using the wecLHS, 10 additional points were added in order to intensify observations at smaller distances and to ensure a spatially distributed coverage of the study area. Figure 1 shows the distribution of the 40 soil moisture monitoring locations (i.e., network nodes) based on the wecLHS.

4.3. Pedological characterization

At each of the 40 pre-defined soil moisture monitoring locations, the soil profile was described down to ca. 60 cm depth and grain size distributions were determined for each node and each soil horizon. Silty loam Cambisols were found to be the dominant soil type, with coarser textured soils on the upper positions on the south-exposed slope and finer textured soils in the valley. With a hydropedological approach (Lin, 2003), soil morphology was described accurately in order to take into account the relevance of hydrological processes as related to soil morphological characteristics and topographic position. Four soil-topographical units (STUs) were identified (Figure 1):

- STU 1: silty loam Cambisol on summit and backslope position, south exposed (slope 2 – 6 %), shallow depth to bedrock, rock fragments, well drained;
- STU 2: silty loam Cambisol in footslope position, evolved on silty colluvial material, south exposed (slope 3 - 8 %); at the depth of ca. 40 cm and deeper, hydromorphic features (such as clay illuviation cutans, clayskins, Fe and Mn coatings) were observed within the Bw and the Bt horizons;
- STU 3: loam and silty loam stagnic Gleysols in the valley bottom, where the thick soil organic matter (SOM)-rich A horizon and the coarser textured BC horizon indicate consistently different hydrologic states compared to the slopes; redox features were observed over the entire soil profile; in wet seasons, the soil was observed to be saturated locally, according to the heterogeneous small scale topography;
- STU 4: silty loam Cambisol on backslope to footslope position, evolved on silty colluvial material, north exposed (slope 5 – 10 %); at the depth of ca. 40 cm and deeper, hydromorphic features (such as clay illuviation cutans, clayskins, Fe and Mn coatings) were observed within the Bw horizon, in concave footslope positions.

Table 1 *- Characterization of the soils at the Schäfertal hillslope site: because of the spatial variability of soil texture shown in Figure 2, we decided to report the median values of grain size in order to represent typical soil texture; bulk density was determined from volumetric soil samples collected at one benchmark soil profile for each STU; porosity was estimated from the maximum measured value of soil water content.*

Soil horizon		Clay [%]	Silt [%]	Sand [%]	BD [g·cm^{-3}]	Porosity [%]
STU 1	AB	17.22	69.48	13.78	1.25	0.50
	Bw1	15.61	70.85	12.79	1.25	0.47
	Bw2	13.86	61.59	25.08	n.a.	0.46
STU 2	AB	16.20	77.54	6.74	1.10	0.55
	Bw	14.80	79.03	6.14	1.36	0.48
	Bt	14.45	75.63	6.40	1.45	0.47
STU 3	A	25.31	66.56	10.20	0.90	0.80
	Bg	15.88	59.16	23.18	1.43	0.75
	BCg	9.24	43.66	47.10	1.53	0.55
STU 4	AB	14.62	76.70	9.07	1.05	0.65
	Bw1	13.75	75.71	11.34	1.34	0.55
	Bw2	11.67	73.39	12.59	1.45	0.45

These STUs represent distinct soil-topography associations that are likely to be representative of different hydrologic responses, enhancing an improved understanding of soil moisture dynamics. In addition to the textural data determined at the positions of each measurement node, for each STU, one representative soil profile was sampled and for each of the three soil horizons the soil bulk density was estimated. Table 1 and Figure 2 provide an overview about the characteristics of each STU and each soil horizon.

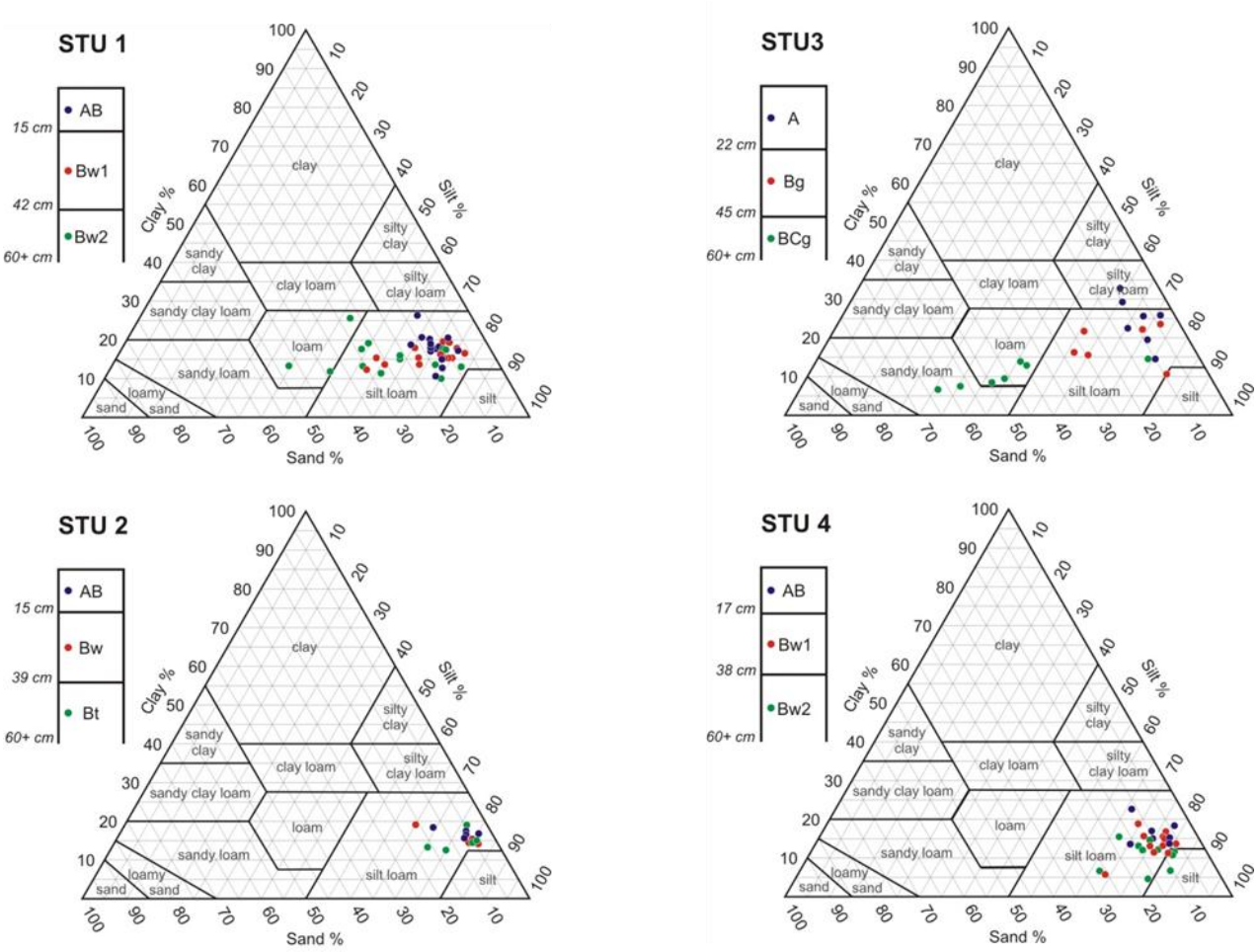

Figure 2 *- Typical textural composition of soil profiles within the depth of 60 cm for each STU, and textural triangles including all soil samples collected for each soil horizon at each of the 40 network nodes. Blue, red and green dots represent topsoil, intermediate and deep horizon, respectively.*

4.4. Soil moisture measurements

Soil moisture (θ) and soil temperature were measured using a so-called hybrid wireless sensor network (SoilNet, Bogena et al., 2010) which includes underground and aboveground devices. Soil moisture sensors are wired to an underground network node, while the aboveground network devices are routers and a coordinator which transmit the data to a computer where it is stored. The network comprises 40 network nodes which were permanently installed at the locations described above (Figure 1). At each network node, six sensors are permanently installed in the soil profile, each with two repetitions at three depths (5, 25 and 50 cm) composing two parallel soil profiles instrumented at each node, with a horizontal distance of ca. 20 cm. The monitoring network measures soil moisture and soil temperature with hourly resolution.. The sensors in use are based on a ring oscillator (SPADE, sceme.de GmbH i.G., Horn-Bad Meinberg, Germany; Hübner et al., 2009). A sensor-specific seven-point-calibration in reference media with well-known dielectric permittivities

(Kögler et al., 2013) was conducted to improve the θ measurement accuracy. Additionally, a sensor-specific temperature calibration was performed.

The spatial distribution of the network nodes covers adequately but not equally all STUs, with 18 nodes distributed in STU 1 and 5, 7 and 12 nodes in STU 2, STU 3 and STU 4, respectively (Figure 1).

The sensor-specific calibration is used to calculate the dielectric number for each measurement from the voltage reading. The complex refractive index model (CRIM) is then used according to Roth et al. (1990) to calculate volumetric soil water content θ (m^3/m^3) using:

$$\theta = \frac{\sqrt{\varepsilon'_c} - \sqrt{\varepsilon'_{matrix}} - \phi\left(\sqrt{\varepsilon'_{air}} - \sqrt{\varepsilon'_{matrix}}\right)}{\sqrt{\varepsilon'_{water}} - \sqrt{\varepsilon'_{air}}}$$

where ε'_c is the bulk dielectric number of the soil composed of soil matrix, water and air, ε'_{matrix} is the dielectric number of the solid matrix of the soil (assumed to be 4.6 for quartz), φ is soil porosity, ε'_{air} is the dielectric number of air (i.e., 1) and ε'_{water} is the dielectric number of water at measurement temperature. Porosity was estimated for each STU and each depth as a fixed value taking into account the maximum θ values observed (Table 1). The resulting porosity values range between 0.45 and 0.8, with lowest values for the deep horizon in the north exposed slope and highest values for the highly organic topsoil in the valley bottom.

The monitoring period analyzed in this study started on 15 September 2012 and ended on 14 November 2013. For each STU, the daily mean soil moisture content (θ_d) was calculated by averaging all measurements collected on a given day over all available network nodes for each depth.

In sensor networks composed by a large number of sensors permanently installed in the soil (Rosenbaum et al., 2012), various causes can result in data loss or produce noisy data and outliers, inclusive unrealistic values. In order to ensure good data quality necessary for statistical analysis, the time series of θ for each sensor were analyzed and compared with their repetition (second sensor at same depth) at the same network node.

At first, unrealistic values (i.e., θ outside the range of 0 to 1 cm^3/cm^3) were removed from the dataset. Values that show a difference of ±0.1 cm^3/cm^3 with the previous reading and correspond to anomalies of the battery and/or temperature voltage were removed. Systematic errors (i.e., θ values that show a difference of ±0.05 cm^3/cm^3 with respect to the previous reading, present at the same time for all the sensors of a single network node) were deleted since this phenomenon can be related to malfunctioning of the end device (i.e., due to abrupt changes in the battery voltage). These qualitative plausibility checks affected 40 % of the sensors. For single sensors showing a systematic offset due to anomalous voltage input (shifting up or down of the readings) a substituting correction of the values was attempted based on the difference with the repetition sensor. In some occasions, linear interpolation of the θ time series was applied. This interpolation was only accepted if the data of the repetition sensor or neighbouring nodes showed no evidence of rainfall, changes in the groundwater level or changes in the evapotranspiration rate (i.e.,

typically for gaps no longer then a few days). Linear interpolation was applied to 16 % of the total number of sensors. For the data analysis, all remaining hourly measurements were assimilated into daily soil moisture (θ_d) values.

4.5. Electromagnetic induction (EMI) measurements

Soil ECa was mapped during 7 campaigns within the monitoring period, using two similar EMI devices. The physical principles behind the sensor functioning can be synthesized as follows: an alternating current flowing in a transmitting coil generates a primary magnetic field (Hp); the field creates an eddy current within the soil, which induces a secondary magnetic field (Hs), which is sensed, together with Hp, by the receiver coil. The secondary magnetic field and the depth of investigation are strongly related to intercoil spacing (s), operating frequency (f) and soil conductivity (σ). The ratio between Hs and Hp, providing to work under the low induction number approximation, is linearly proportional to the soil ECa (McNeill, 1980). The cumulative depth-response of the instrument is a non-linear function and varies between vertical dipole mode (VDP, coils perpendicular to the soil) and horizontal dipole mode (HDP, coils parallel to the soil). In the ideal case of homogeneous soil material, the major contribution to the ECa sensed in VDP will refer to the depth of ca. 0.4·s (i.e. 40 % of the coil spacing), with a maximum depth of investigation of 1.5·s. For the HDP mode, the maximum depth of investigation is 0.75·s, with major contribution from the soil surface (McNeill, 1980).

For the present work, two devices were tested: EM38-DD and EM38-MK2 (Geonics Ltd., Ontario, Canada). The EM38-DD is composed by two units mounted perpendicularly to each other, both consisting of transmitter and a receiver coil spaced 1 m. This allows measuring the ECa at two depths at the same time for every measurement location. The measured data for the two dipole configurations have a different sensibility response, which results, for the VDP, in a maximum sensibility corresponding to ca. 0.20 and 0.40 m (respectively for the two intercoil spacings) and a maximum survey depth corresponding to ca. 0.75 and 1.50 m (respectively for the two intercoil spacings), given the operating frequency of 14.5 kHz.

The EM38-MK2 is composed by one unit, which can operate either in HDP or VDP at the frequency of 14.6 kHz. Two receiver coils spaced respectively 0.5 and 1.0 m from the transmitter coil allow measuring ECa within the soil depth of 0-0.37 and 0-0.75 m (respectively, for the HDP), and 0-0.75 and 0-1.50 m (respectively, for the VDP).

The main advantage of the EMI surveys is that the induction principle does not require a direct contact with the ground. Consequently a survey carried out using EMI sensors can be faster than an equivalent survey carried out with other instruments. The survey can be performed by a single operator, while a GPS receiver, connected to the instrument, allows collecting georeferenced ECa data.

4.6. ECa data processing

For each of the 7 measurement dates, 4 datasets of ECa were collected: EM38-DD_{HDP} EM38-DD_{VDP}, EM38-$MK2_{HDP(s=0.5m)}$ and EM38-$MK2_{HDP(s=1.0m)}$. The surveys were conducted mounting the EMI device on a sledge (made of wood and plastic, in order to avoid conductivity

anomalies) and carried by one operator at constant walking speed. For each measurement date, the study area was first surveyed using the EM38-DD and, later, using the EM38-MK2.

The study area was divided into 3 fields: northern slope, valley floor and southern slope, and each of them was measured separately; the duration of the survey of such subareas was ca. 45 minutes for the northern slope, 15 minutes for the valley floor and ca. 30 minutes for the southern slope. A unique location, beside the study area, was used as calibration point, i.e. instrument nulling (McNeill, 1980) before each survey, and according to the recommendations of, e.g. Robinson et al. (2004), a warm-up period was ensured before the actual measurements. Before and after each survey, ECa was measured along a reference profile (i.e. a specific 40 m-transect transect) in order to assess and correct possible drift within the data (e.g. Sudduth et al., 2001; Abrahamet al., 2006). ECa was measured along survey lines spaced 5 m; along each survey line, ECa was samples with a rate of 5 records/s, thus with an approximate resolution of ca. 0.2 m. Towards the end of each survey, crossing lines (Simpson et al. 2009) were measured in order to use the cross-over points for drift correction (Delafortrie et al., 2014); one example is shown in Figure 4.

Generally, all the datasets were found to provide similar spatial pattern of ECa. Data collected using the EM38-MK2 as well as the EM38-DD_{HDP} showed large noise. We attribute this fact to the presence of a big volume of grass (sometimes wet) on the surface, which can interfere with the inductive process. This data noise causes critical problems in data processing and hindered a purposeful data interpretation. As the datasets of EM38-DD_{VDP} showed neither significant noise nor drift, only those data were used for the present work.

The data were checked for outliers, which can occur when ECa was measured over one of the nodes of the soil moisture and soil temperature monitoring network, or by accidental errors during the survey.

Temperature correction was performed according to the correction factors provided in USDA (1954) According to the already mentioned sensitivity function of the device EM38-DD in VDP, the available soil temperature values at the depths of 25 and 50 cm were averaged and used for calibration: three different soil temperature values were calculated: one for the valley floor and one for the two slopes with opposite exposition, respectively.

4.7. Statistical analysis of the characteristic states of soil moisture (Martini et al, submitted)

Similar to the hypothesis of preferred states, which was explained in detail by Grayson et al. (1997), we hypothesized two soil moisture states to be characteristic for the Schäfertal site.

We define a *wet state* for the period during which precipitation exceeds evapotranspiration and a connection between adjacent parts of the hillslope is possible due to the dominance of lateral water movement with respect to vertical fluxes. Lateral flow in the subsurface is expected to take place along the slopes, where the architecture of soil horizons allows it. Soil moisture is higher than the annual mean everywhere, although convergent areas such as the valley bottom show higher soil water content compared to backslope areas. Topography and aspect play a dominant role, in conjunction with local soil properties, in determining the spatial organization of soil moisture.

In a similar manner, we define a *dry state* for the period characterized by reverse relative importance of meteorological inputs. During this period, evapotranspiration exceeds precipitation, and vertical water fluxes are dominant: water from precipitation infiltrates slowly into the soil, due to low hydraulic conductivity associated with low soil water content, and may rapidly be removed by evapotranspiration after the rainfall ends. During this state, soil moisture patterns are governed only by local soil properties, while lateral connections are inactive between different areas of the slopes. These two characteristic states were denoted by Grayson et al. (1997) as *nonlocal* and *local control*, respectively.

At the Schäfertal site, we expect the wet state to be present in the winter period, when the overall mean soil water content is relatively stable at high values close to field capacity and snow coverage may be present. At the beginning of the spring, rainfall events are typically strong, evapotranspiration increases and the snow (if present) melts. During this period of high inputs, different patterns may be established: lateral redistribution of soil moisture takes place and convergent areas are likely to reach saturation, eventually facilitating overland flow as observed sometimes within the Schäfertal catchment. When the intense rainfall period ends, evapotranspiration acts as major control while lowering the spatial mean soil moisture until the dry state is reached. At this stage, rainfall events can wet the topsoil only for short periods of time, because plant activity, solar radiation and high air temperature facilitate the fast evapotranspiration from the topsoil. At the end of the summer period, evapotranspiration decreases and precipitation increases, thus the soil wets progressively until the wet state is reached again.

The persistence of soil moisture spatial organization can be analyzed by calculating the Spearman rank correlation coefficient rs. According to Vachaud et al. (1985), it is defined as

$$r_s = 1 - 6 \sum_{i=1}^{N} \frac{(R_{si} - R_{sj})^2}{N(N^2-1)}$$

where R_{si} is the rank of the soil moisture observation θ_{si} for the sensor s and for the day i, and R_{sj} is the rank of the soil moisture observation for the same sensor, but for the day j. Such a coefficient (ranging between -1 and 1) is a measure of statistical dependence between two variables (i.e., two daily data sets): $r_s = 1$ when there are no changes in the rank of the soil moisture observations and decreases in r_s occur proportionally to the number of observations for which the rank varies and the number of position changed both toward a higher or lower rank. The r_s coefficient is widely used as a measure of similarity of soil moisture patterns for campaign-based and for temporal stability studies, with the aim of finding locations which best represent the spatial mean soil moisture of a given site (e.g., Martínez-Fernández and Ceballos, 2005; Brocca et al., 2010).

For this study, the change in rs was calculated with respect to the ranked mean soil moisture (θ_d) values of the reference dates for the wet and for the dry states. In such a manner, two time series of r_s were calculated, showing for each day the degree of similarity to the reference wet (r_{sW}) and the reference dry state (r_{sD}), respectively. It is important to notice that a high value of r_s does not imply that the magnitude of changes in individual soil moisture values is low, but rather that they do not induce a change in the spatial soil moisture pattern. In fact, it does not account for the quantitative aspect unless it results in changes of the rank. Therefore the r_s coefficient has to be considered as a qualitative

representation of the similarity between the spatial pattern of soil moisture for a given day referred to the wet or to the dry state.

For this analysis, sensors with missing θ_d values were discarded and only sensors having daily values (θ_{ds}) for the complete monitoring period were evaluated. For this reason, a subset of network nodes (i.e., 16 benchmark nodes composed of 48 sensors distributed over three depths) was selected according to the completeness of the time series (i.e., no missing θ_{ds} values), and to the spatial location (Figure 1). For each STU, the daily mean soil moisture calculated using the benchmark profiles was tested to be correlated well with the values calculated using all the sensors.

In order to evaluate the effect of soil water content on ECa detected by the EM38-DD survey, one value of ECa for each location corresponding to the nodes of the soil moisture and soil temperature monitoring network was extracted from the dataset of each measurement date. A weighted function within the radius of 15 m was applied, with major contribution provided by the 0-3 m distance.

For each EMI survey date, a dataset of θ was extracted, and linear regression and coefficient of determination (R^2) between ECa and θ was calculated for each depth at which soil moisture was monitored. Additionally, the qualitative similarity of spatial patterns of ECa and θ was evaluated through the r_s coefficient.

Antecedent precipitation (AP5) was calculated for every EMI survey date as the sum of daily precipitation during the previous 5 days.

5. Results

5.1. Description of characteristic states of soil moisture using a wireless soil moisture sensing network

The daily average hillslope soil moisture for the depths 5, 25 and 50 cm is shown in Figure 3d, together with the above mentioned time series of precipitation (P) and potential evapotranspiration (PET) over the monitoring period. From September to end of December 2012, PET decreases progressively and θ_d increases stepwise after each rainfall event. In mid-December, the first snowmelt took place; an average snow height of 26 cm was measured at 55 positions within the study area on December 13th. During the winter period (January to March 2013), P and PET were relatively low and little changes of daily mean soil moisture were determined by precipitation events of longer duration. The winter period shows low temporal variability of daily mean soil moisture: convergent areas remain at or near field capacity, and rainfall events produce i) on the hillslopes an increase of soil moisture which is then redistributed both vertically and laterally ii) near-saturation to saturation at the footslope and in the valley bottom. Snow covered the soil surface for most of the winter period.

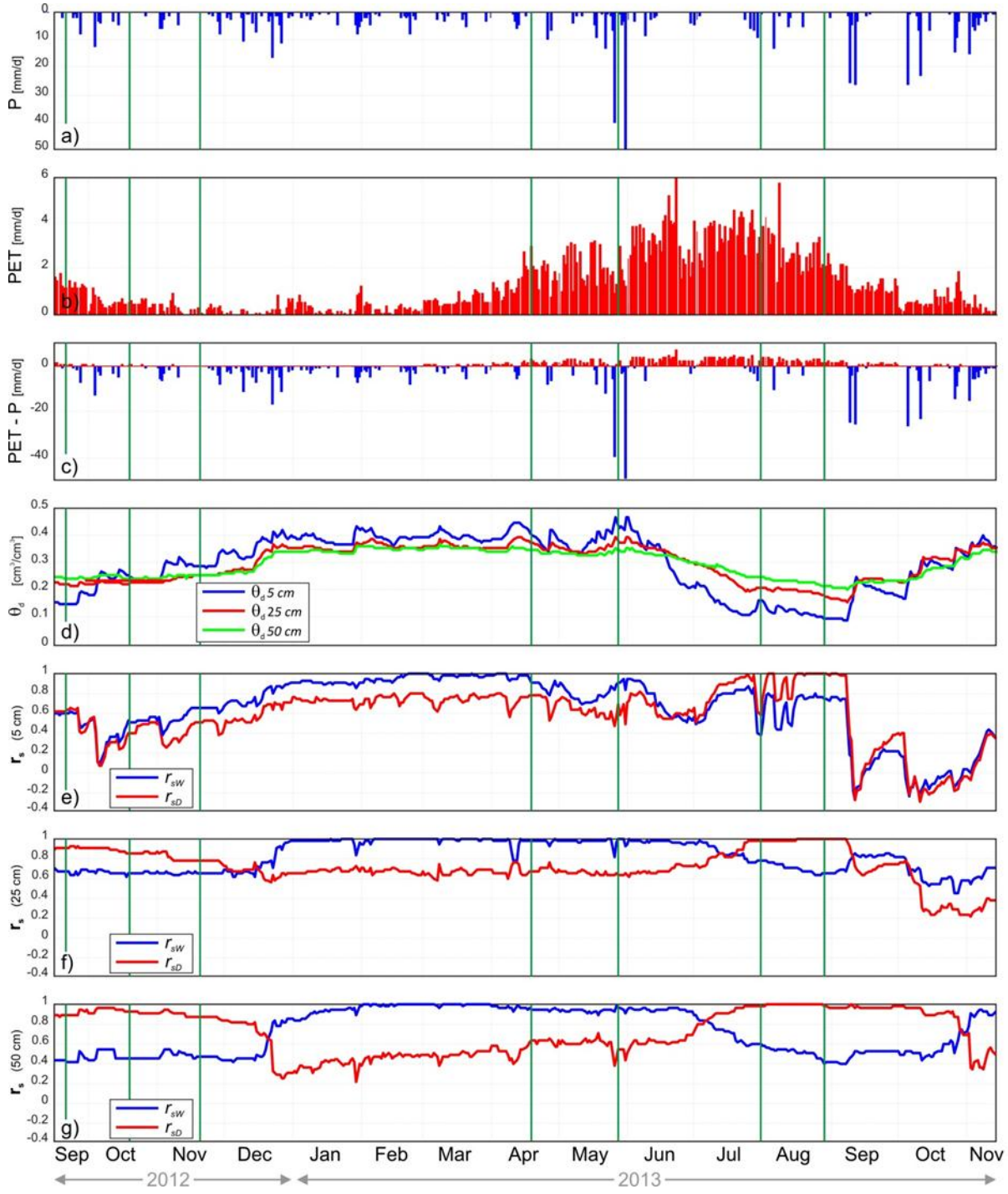

Figure 3 *- Time series of a) precipitation (P); b) potential evapotranspiration (PET); and c) P – PET; d) hillslope daily averaged soil water content (ϑ_d) for the three depths of investigation; e) r_{sW} and r_{sD} for the 5 cm depth; f) r_{sW} and r_{sD} for the 25 cm depth; g) r_{sW} and r_{sD} for the 50 cm depth. For each day, r_{sW} was calculated as referred to February 28th, 2013 (as being representative of the characteristic wet state by showing the minimum deviation from the hillslope average soil moisture during the winter period), and r_{sD} was calculated as referred to August 25th, 2013 (as being representative of the characteristic dry state by showing the minimum deviation from the hillslope average soil moisture during the summer period). Green vertical lines indicate the dates of EMI surveys.*

In March, PET started to increase gradually but P input remained low, and θ_d remained at the characteristic wet state until April 6th, when the snowmelt started. At this point, atmospheric forcing (i.e., frequent rainfalls and increasing PET) determined rapid wetting and drying cycles of the topsoil. Between May 17th and 31st, 2013, intense rainfalls (total P = 137 mm, with max P = 50 mm/d on May 31st) wetted the soil until the maximum observed hillslope average soil moisture of 0.46 cm^3/cm^3 was reached. During those days, large part of Central Europe was flooded. At the study site, saturation excess overland flow was observed and riparian areas remained saturated for several days. Afterwards, high PET and low P allowed the drying phase to be established, bringing the topsoil average soil moisture below 0.1 cm3/cm3, θ_d,25 and θ_d,50 to 0.15 and 0.20 cm^3/cm^3, respectively, at the beginning of September 2013.

It can be noticed in Figure 3d that after the end of July the drying rate decreased, according to the reduction of PET and the occurrence of a few precipitation events (max summer P = 13.6 mm/d on August 6th), which only wetted the topsoil. Following two intense rainfalls at the beginning of September (P = 25.6 mm/d on September 9th; P = 26.2 mm/d on September 11th, 2013) the topsoil average soil moisture increased by 0.16 cm^3/cm^3 (from 0.09 on September 8th to 0.25 cm3/cm3 on September 12th, 2013). After rapid drying of the topsoil, the wetting phase started with two similar events on October 5th (P = 26.6 mm/d) and 11th (P = 23.4 mm/d).

Based on the time series of daily mean soil moisture θ_d (Figure 3d), the wet state is assumed to be present between the end of December 2012 and the beginning of April 2013. More precisely, we selected the beginning of the period to be five days after the last rainfall event with P > 10mm/d (observed on December 27th, 2012) and the end to coincide with the observed snow melt (which started on April 6th, 2013 with a rain-on-snow event). During this period (94 days in total), the standard deviation of daily mean soil moisture for the depth of 5, 25 and 50 cm is 0.016, 0.011 and 0.008 cm3/cm3, respectively. Similarly, the dry state was assumed to occur between August 12th (five days after a rainfall event with P = 13.6 mm/d) and September 8th, 2013 (P = 25.6 mm/d). The calculated standard deviation is 0.013, 0.014 and 0.010 cm3/cm3 for the three soil depths at which soil moisture was measured.

For each time interval, the mean soil moisture for each depth and each STU was calculated, and compared with the daily mean soil moisture of each STU. The date with smallest cumulative deviation from the mean (i.e., the sum of absolute values of deviations for all STUs and all depths) was selected as representative for the wet state. With the same criteria, the reference date for the dry state was selected. The dates of February 28th and August 25th, 2013 were found to be representative for the wet and dry characteristic states of soil moisture, respectively.

5.2. Suitability of repeated EMI surveys to map spatial patterns of soil moisture dynamics

The study site showed overall low values of ECa compared to other studies (e.g. Robinson et al., 2004; Zhu et al., 2010; Robinson et al., 2012; Priori et al., 2013; Delefortrie et al., 2014), spread within a small range (Table 2).

Although θ_d varies at the depths of 25 and 50 cm, which contribute largely to the bulk ECa signal (McNeill, 1980); variations in the range of ECa do not reflect variations in the range of θ_d.

The overall spatial pattern of ECa does not differ substantially between the survey dates; therefore only one example dataset is shown in Figure 4. The highest values of ECa were measured in the valley bottom (STU 3) and footslope positions (STU 2), while backslope areas (STU1 and STU4) show low ECa values.

Table 2 *- Statistics of the 7 EMI surveys based on the 40 network nodes; the Spearman rank correlation coefficient (r_s^{DATE}) was calculated between each dataset and every other dataset in order to characterize the similarity of spatial patterns of ECa; antecedent precipitation (AP5) was calculated as the sum of rainfall amounts during the 5 days before each survey date; the coefficient of determination $R^2_{EMI\text{-}AP5}$ refers to the linear regression between the series of Spearman correlation for each survey date (rsDATE)and AP5.*

	19-Sep-2012	18-Oct-2012	20-Nov-2012	18-Apr-2013	28-May-2013	31-Jul-2013	29-Aug-2013
average ECa [mS/m]	9.59	7.15	9.20	11.28	8.30	7.69	6.32
ECa range [mS/m]	4.21	11.04	8.22	10.01	3.97	4.46	9.91
$\theta_{d,5}$ [m^3/m^3]	0.15	0.26	0.29	0.41	0.43	0.16	0.10
$\theta_{d,25}$ [m^3/m^3]	0.22	0.22	0.25	0.37	0.37	0.21	0.17
$\theta_{d,50}$ [m^3/m^3]	0.24	0.24	0.25	0.35	0.35	0.25	0.23
range $\theta_{d,5}$ [m^3/m^3]	0.18	0.33	0.32	0.51	0.47	0.21	0.17
range $\theta_{d,25}$ [m^3/m^3]	0.28	0.32	0.29	0.53	0.37	0.50	0.33
range $\theta_{d,50}$ [m^3/m^3]	0.35	0.35	0.36	0.50	0.36	0.44	0.53
r_s^{SEP12}	1	0.70	0.59	0.82	0.17	0.53	0.86
r_s^{OCT12}	0.70	1	0.90	0.93	0.65	0.94	0.86
r_s^{NOV12}	0.59	0.90	1	0.84	0.73	0.97	0.71
r_s^{APR13}	0.82	0.93	0.84	1	0.52	0.85	0.91
r_s^{MAY13}	0.17	0.65	0.73	0.52	1	0.82	0.51
r_s^{JUL13}	0.53	0.94	0.97	0.85	0.82	1	0.75
r_s^{AUG13}	0.86	0.86	0.71	0.91	0.51	0.75	1
AP5 [mm]	2.80	5.12	0.47	1.50	50.00	17.40	0.40
$R^2_{EMI\text{-}AP5}$	0.77	0.34	0.02	0.81	0.51	0.01	0.72

The correlation between ECa and θ_d for the locations where soil moisture was monitored is shown in Figure 5. Interestingly, clear positive correlations were found for the surveys carried out in April, July and August 2013 (and partially for September 2012), but not for the remaining datasets. In terms of absolute soil moisture, thus, the spatial distribution of ECa was found to be strongly related to the spatial distribution of soil moisture for one of the two surveys under wet conditions (April 2013, near field capacity conditions). Under dry conditions (July and August 2013), a generally good correlation (either R2 or rs) was found, except for the topsoil in July 2013. For the first three survey dates (during the transition towards the wet state, in September, October and November 2012) a rather poor correlation was found, except for ECa-September 2012 against $\theta_{d,25}$. Such situation may be clarified referring to the hydrological processes which were described as controls for the spatial pattern of soil moisture (Figure 3), and taking into account the antecedent precipitation (AP5 in Table 2).

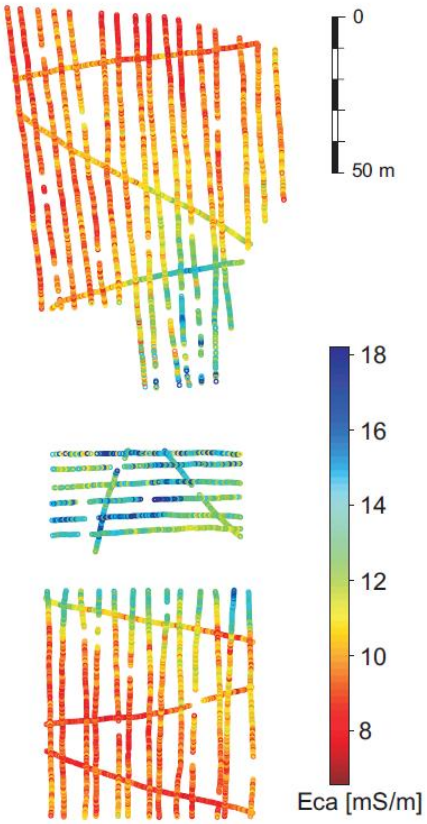

Figure 4 *- Example dataset of ECa, measured on October 18th, 2012.*

Highest correlation between ECa and θ_d refers to survey dates, under either wet or dry conditions, with low AP5. In other words, ECa shows poor correlation with θ_d during wetting periods, such as after intense rainfall events. In fact, at these times, water movement is more strongly affected by topography which facilitates accumulation of water towards depressions than by local soil properties only. Such condition is described as nonlocal control by Grayson et al. (1997). Spatial distribution of ECa can explain well the spatial distribution of soil moisture when local redistribution, rather than wetting, is dominant, e.g. under dry soil conditions, or after the nonlocal control exerted its effect, and the local control becomes dominant (Grayson et al., 1997). In fact, EMI surveys in the wet state show strong correlation to soil moisture for April 2013, i.e., a few days after precipitation ended but not for May

2013, within an extreme precipitation event that caused severe floods. And, in the dry state, poor correlation was found for July 2013, i.e. immediately after rainfall (which, as expected, appears to influence only the spatial pattern of soil moisture in the topsoil as shown in Figure 3e-g), while strong positive correlation was found for August 2013, with AP5 close to zero. The relation between ECa and θ_d for the wetting transition (September, October and November 2012) seems to be unclear, due to the continuous reorganization of the spatial pattern of soil moisture (Figure 3e-g) caused by rainfall events (Figure b) associated with the reduction of evapotranspiration (Figure 3a).

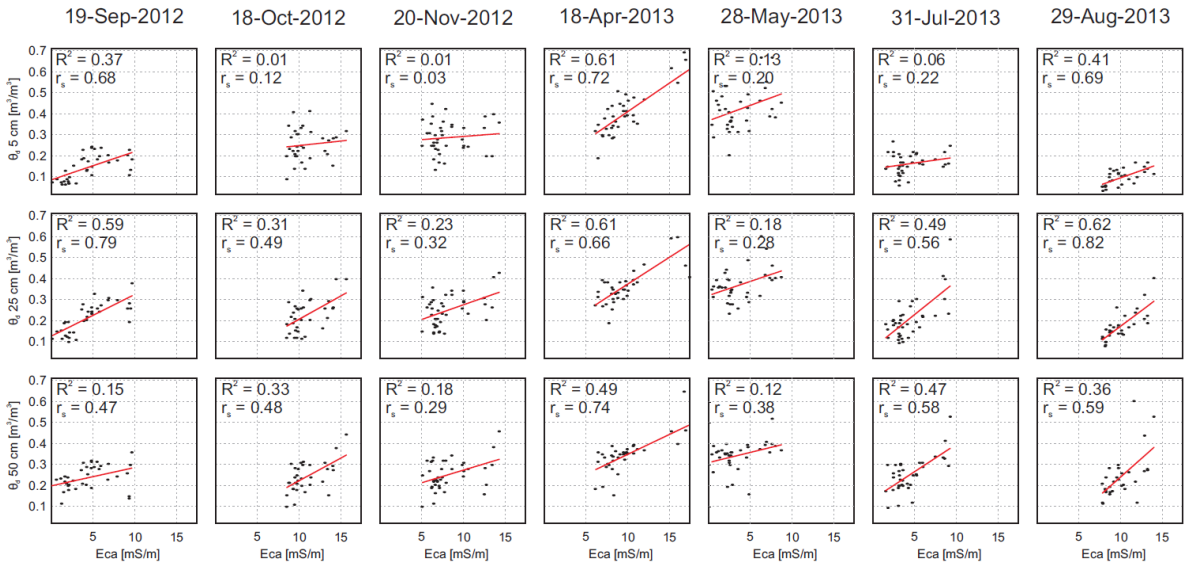

Figure 5 *- Correlation between ECa and ϑ_d: for every date of EMI survey, a linear regression was fitted between the ECa values extracted for the 40 network nodes and the daily mean soil water content at the depths of 5, 25 and 50 cm, measured by the soil moisture and soil temperature monitoring network. For each plot, the coefficient of regression (R^2) and the spearman rank correlation coefficient (r_s) are indicated.*

6. Discussion and conclusion

In the present work, a combination of wireless soil moisture sensing network and mobile geophysical measurements to characterize the soil moisture dynamics and their relation with site characteristics such as soil properties, topography and atmospheric forcing for a grassland hillslope area was tested. Through the analysis of in situ measurements from a soil moisture sensor network, we described the spatial and temporal evolution of soil moisture patterns, and inferred hydrological processes controlling such evolution. Results will in future help to improve conceptual models for hydrological studies at similar or smaller scales, as well as to transfer observation concepts and process understanding to larger or less instrumented areas.

The soil moisture monitoring network provided a dataset of hourly measurements for 240 sensors distributed at three fixed depths. Such large dataset required statistical tools for extracting the most relevant information. We proposed a method based on the Spearman rank correlation coefficient as a measure of similarity between the spatial distribution of soil moisture for a certain date and two reference patterns. The method showed to provide

valuable insight into the persistence of characteristic soil moisture states and the mechanisms of transitions between such states. Additionally, the method showed to be suitable for highlighting events, for which specific hydrological processes occurred. For instance, preferential flows through the topsoil in the valley bottom were detected as abrupt declines of both the r_{sW} and r_{sD} coefficients for the 5 cm depth. It is important to remark that the r_s coefficient can only provide a qualitative measure of similarity, because changes of absolute values of soil water content do not influence the value of the coefficient unless they induce changes in the rank of the observations. For the same reason, even when changes of r_s occur, there is no information on the magnitude of change in soil water content.

Soil moisture patterns of the topsoil were observed to be very dynamic, being the soil surface prompt to spatial reorganization as effect of atmospheric boundary conditions. The persistence of the characteristic soil moisture patterns was limited: intense rainfall events changed the spatial pattern of soil moisture in the topsoil especially under initially dry conditions, and preferential flow in the valley bottom played the major role in the reorganization of the soil moisture pattern. A decreasing variability of the spatial organization of soil moisture with depth was observed. The intermediate soil horizon showed more stable patterns, being the wet and dry characteristic states of soil moisture able to describe the spatial pattern of soil moisture at the depth of 25 cm for most of the monitoring period. At this depth, preferential flow occurring under initially dry conditions, led to the most significant changes of the spatial pattern of soil moisture, with effects that persisted for several months during the observed period of time. The deep soil horizon was described well by either the wet or the dry characteristic states of soil moisture: small dynamics were observed during the monitoring period, and switches were observed to occur very rapidly.

With the aim of mapping soil moisture and its dynamics at the hillslope scale, using state-of-the-art sensor technologies and efficient statistical methods, widely used proximal soil sensing such as electromagnetic induction methods are expected to be a suitable alternative to the emerging wireless sensor technology. Nevertheless, the results of the combined investigation that we conducted suggest the need for an accurate previous understanding of the hydrological behaviour of the site. At the test site used in this study, bulk electrical conductivity showed to represent significantly the spatial distribution of soil moisture only during periods when local soil properties play the major role in determining water distribution within the soil; instead, when water movements are strongly influenced by additional factors (e.g. topography), electromagnetic induction surveys do not provide a suitable tool for mapping the soil's moisture. Our results suggest that such technique is excellent for mapping soils spatial distribution at the field scale, being fast and noninvasive, and able to provide large amount of data with relatively brief surveys. Nevertheless, the link to soil water content seems to be an indirect relation through soil properties. Consequently, we recommend accounting for underlying hydrological processes and pedological expertise, as they both are needed for a consistent interpretation of the geophysical data.

Our results show that a variety of hydrological processes takes place at different times and at different topographic positions, according to local soil properties. The same is true for different soil horizons, when looking at vertical patterns. Such fact has implications for mapping soil moisture from the field to the catchment scale, where the topsoil's moisture does not necessarily mirror processes that take place within the soil profile.

7. References

Abraham, J.D., M. Deszcz-Pan, D.V. Fitterman, B.L. Burton. 2006. Use of a handheld broadband EM induction system for deriving resistivity depth images. Symposium on the Application of Geophysics to Engineering and Environmental Problems, pp. 1782–1799.

André, F., C. van Leeuwen, S. Saussez, R. Van Durmen, P. Bogaert, and D. Moghadas. 2012. High-resolution imaging of a vineyard in south of France using ground penetrating radar, electromagnetic induction and electrical resistivity tomography. J. of Applied Geophysics 78:113–122. doi:10.1016/j.jappgeo.2011.08.002.

Becker A., and J.J. McDonnell. 1998. Topographical and ecological controls of runoff generation and lateral flows in mountain catchments. Hydrology, Water Resources and Ecology in Headwaters: 199-206. Bogena H.R., Huisman J.A., Oberdorster C., Vereecken H. 2007. Evaluation of a low-cost soil water content sensor for wireless network applications. Journal Of Hydrology 344:32-42. DOI: Literatur06.

Bogena, H., M. Herbst, J.A. Huisman, U. Rosenbaum, A. Weuthen, and H. Vereecken. 2010. Potential of wireless sensor networks for measuring soil water content variability. Vadose Zone J.l 9:1002-1013. doi:10.2136/vzj2009.0173.

Borchardt D. 1982. Geoökologische Erkundung und hydrologische Analyse von Kleineinzugsgebieten des unteren Mittelgebirgsbereichs, dargestellt am Beispiel der oberen Selke, Harz. (In German). Petermanns Geographische Mitteilungen 82:251-262.

Brocca L., F. Melone, T. Moramarco, R. Morbidelli. 2010. Spatial-temporal variability of soil moisture and its estimation across scales. Water Resources Research 46. DOI: Artn W02516.

Corwin D.L., and S.M. Lesch. 2005. Apparent soil electrical conductivity measurements in agriculture. Computers And Electronics In Agriculture 46:11-43. DOI: DOI 10.1016/j.compag.2004.10.005.

Cousin, I., A. Besson, H. Bourennane, C. Pasquier, B. Nicoullaud, D. King, and G. Richard. 2009. From spatial-continuous electrical resistivity measurements to the soil hydraulic functioning at the field scale. C. R. Geosci. 341:859–867. doi:10.1016/j.crte.2009.07.011.

Samuël D., P. De Smedt, T. Saey, E. Van De Vijver, M. Van Meirvenne. 2014. An efficient calibration procedure for correction of drift in EMI survey data. J. of Applied Geophysics 110: 115-125. doi:10.1016/j.jappgeo.2014.09.004.

Dierke, C., and U. Werban. 2013. Relationships between gamma-ray data and soil properties at an agricultural test site. Geoderma 199: 90-98. doi:10.1016/j.geoderma.2012.10.017.

Doolittle, J.A., and E.C. Brevik. 2014. The use of electromagnetic induction techniques in soils studies. Geoderma 223–225: 33–45. doi:10.1016/j.geoderma.2014.01.027.

Doolittle, J.A., S.J. Indorante, D.K. Potter, S.G. Hefner, and W.M. McCauley. 2002. Comparing three geophysical tools for locating sand blows in alluvial soils of southeast Missouri. J. Soil Water Conserv. 57:175–182.

Fertl, W.H. 1979. Gamma ray spectral data assist in complex formation evaluation. The Log Analyst. 3-37.

Grayson R., and G. Blöschl. 2001. Spatial patterns in catchment hydrology : observations and modelling Cambridge University Press, Cambridge, U.K. ; New York.

Grayson, R.B., A.W. Western, F.H.S. Chiew, and G. Blöschl. 1997. Preferred states in spatial soil moisture patterns: Local and non-local controls. Water Resources Research, 33(12): 2897-2908. doi:10.1029/97WR02174.

Hansen B. 2005. Wireless sensor network helps prevent water, soil pollution. Civil Engineering 75:34-35.

Hübner, C., R. Cardell-Oliver, R. Becker, K. Spohrer, K. Jotter, and T. Wagenknecht. 2009. Wireless soil moisture sensor networks for environmental monitoring and vineyard irrigation. In: 8th International Conference on Electromagnetic Wave Interaction with Water and Moist Substances (ISEMA 2009), Helsinki, Finland. pp.408–415.

Huth N.I., and P.L. Poulton. 2007. An electromagnetic induction method for monitoring variation in soil moisture in agroforestry systems. Australian Journal of Soil Research 45:63-72. DOI: Doi 10.1071/Sr06093.

Kachanoski R.G., E.G. Gregorich, I.J. Vanwesenbeeck. 1988. Estimating Spatial Variations of Soil-Water Content Using Noncontacting Electromagnetic Inductive Methods. Canadian Journal of Soil Science 68:715-722.

Kögler, S., F. Schmidt, E. Martini, J. Bumberger, S. Zacharias, and U. Wollschläger. 2013. Comparison of two calibration approaches for low-cost soil moisture sensors. In: 7th CMM Conference 2013 Innovative Feuchtemessung in Forschung und Praxis, Krlsruhe, Germany, 24th September 2013.

Martínez-Fernández, J., and A. Ceballos. 2005. Mean soil moisture estimation using temporal stability analysis. J. Hydrology 312:28-38.

Martini, E., C. Comina, S. Priori, and E.A.C. Costantini. 2013. A combined geophysical-pedological approach for precision viticulture in the Chianti hills. Bollettino di Geofisica Teorica ed Applicata 54(2):165-181. doi:10.4430/bgta0079

Martini E., U. Wollschlager, S. Kögler, T. Behrens, P. Dietrich, F. Reinstorf, K. Schmidt, M. Weiler, U. Werban, S. Zacharias. Spatial and temporal dynamics of hillslope-scale soil moisture patterns: Characteristic states and transition mechanisms. Vadose Zone J (submitted).

McNeill, J.D. 1980. Electromagnetic terrain conductivity measurement at low induction numbers. Tech. Note TN-6, Geonics Ltd., Mississauga, ON, Canada.

Minasny, B., A.B. McBratney. 2006. A conditioned Latin hypercube method for sampling in the presence of ancillary information. Computers & Geosciences 32:1378-1388.

Moghaddam M., D. Entekhabi, Y. Goykhman, K. Li, M.Y. Liu, A. Mahajan, A. Nayyar, D. Shuman, D. Teneketzis. 2010. A Wireless Soil Moisture Smart Sensor Web Using Physics-Based Optimal Control: Concept and Initial Demonstrations. Ieee Journal of Selected Topics in Applied Earth Observations and Remote Sensing 3:522-535. DOI: Doi 10.1109/Jstars.2010.2052918.

Mohanty B.P., and T.H. Skaggs. 2001. Spatio-temporal evolution and time-stable characteristics of soil moisture within remote sensing footprints with varying soil, slope, and

vegetation. Advances in Water Resources 24:1051-1067. DOI: Doi 10.1016/S0309-1708(01)00034-3.

Ollesch G. 2008. Erfassung und Modellierung der Schneeschmelzerosion am Beispiel der Kleineinzugsgebiete Schäfertal (Deutschland) und Lubazhinkha (Russland) Fakultät für Geowissenschaften, Geotechnik und Bergbau TU Bergakademie Freiberg, Freiberg.

Priori, S., E. Martini, and E.A.C. Costantini. 2010 Three proximal sensors for mapping skeletal soils in vineyards. In: R.J. Gilkes and N. Pragonkep, editors, Soil Solutionsfor a Changing World: 19th World Congress of Soil Science, Brisbane, QLD, Australia, 1-6 August 2010. [CD] IUSS.

Priori, S., E. Martini, M.C. Andrenelli, S. Magini, A.E. Agnelli, P. Bucelli, M. Biagi, S. Pellegrini, and E.A.C. Costantini. 2013. Improving wine quality through harvest zoning and combined use of remote and soil proximal sensing. Soil Sci. Soc. Am. J. 77:1338-1348. doi:10.2136/sssaj2012.0376.

Ritsema C.J., H. Kuipers, L. Kleiboer, E. van den Elsen, K. Oostindie, J.G. Wesseling, J.W. Wolthuis, P. Havinga. 2009. A new wireless underground network system for continuous monitoring of soil water contents. Water Resources Research 45. DOI: Artn W00d36.

Robinson, D.A., Lebron, I., Lesch, S.M., Shouse, P., 2004. Minimizing drift in electrical conductivity measurements in high temperature environments using the EM-38. Soil Sci. Soc. Am. J. 68, 339–345.

Robinson D.A., C.S. Campbell, J.W. Hopmans, B.K. Hornbuckle, S.B. Jones, R. Knight, F. Ogden, J. Selker, O. Wendroth. 2008. Soil Moisture Measurement for Ecological and Hydrological Watershed-Scale Observatories: A Review. Vadose Zone J 7:358-389. DOI: Digital06.

Robinson D.A., H. Abdu, I. Lebron, S.B. Jones. 2012. Imaging of hill-slope soil moisture wetting patterns in a semi-arid oak savanna catchment using time-lapse electromagnetic induction. Journal of Hydrology 416:39-49. doi:10.1016/j.jhydrol.2011.11.034.

Romano N. 2014. Soil moisture at local scale: Measurements and simulations. J. Hydrol. doi: 10.1016/j.jhydrol.2014.01.026.

Rosenbaum, U., J.A. Huisman, A. Weuthen, H. Vereecken, and H.R. Bogena. 2010. Sensor-to-Sensor Variability of the ECHO EC-5, TE, and 5TE Sensors in Dielectric Liquids. Vadose Zone J. 91:181. doi:10.2136/vzj2009.0036.

Roth, K., R. Schulin, H. Fluhler, and W. Attinger. 1990. Calibration of time domain reflectometry for water content measurement using a composite dielectric approach. Water Resour. Res. 26:2267–2273.

Savva Y., K. Szlavecz, D. Carlson, J. Gupchup, A. Szalay, and A. Terzis. 2013. Spatial patterns of soil moisture under forest and grass land cover in a suburban area, in Maryland, USA. Geoderma 192:202-210. doi:10.1016/j.geoderma.2012.08.013.

Schmidt, K., T. Behrens, J. Daumann, L. Ramirez-Lopez, U. Werban, P. Dietrich, and T. Scholten. 2014. A comparison of calibration sampling schemes at the field scale. Geoderma 232-234:243-256. doi: 10.1016/j.geoderma.2014.05.013

Scull P., J. Franklin, O.A. Chadwick, and D. McArthur. 2003. Predictive soil mapping: a review. Progress in Physical Geography 27:171-197. doi:10.1191/0309133303pp366ra.

Simpson, D., M. Van Meirvenne, T. Saey, H. Vermeersch, J. Bourgeois, A. Lehouck, L. Cockx, and U.W.A. Vitharana. 2009. Evaluating the multiple coil configurations of the EM38DD and DUALEM-21S sensors to detect archaeological anomalies. Archaeol. Prospect. 16, 91–102.

Sudduth, K.A., S.T. Drummond, N.R. Kitchen. 2001. Accuracy issues in electromagnetic induction sensing of soil electrical conductivity for precision agriculture. Comput. Electron. Agric. 31, 239–264.

Sudduth, K.A., N.R. Kitchen, W.J. Wiebold, W.D. Batchelor, G.A. Bollero, and D.G. Bullock. 2005. Relating apparent electrical conductivity to soil properties across the north-central USA. Comput. Electron. Agric. 46:263–283. doi:10.1016/j.compag.2004.11.010

Terzis A., R. Musaloiu-E, J. Cogan, K. Szlavecz, A. Szalay, J. Gray, S. Ozer, C.J.M. Liang, J. Gupchup, and R. Burns. 2010. Wireless sensor networks for soil science. International Journal of Sensor Networks 7:53-70.

Triantafilis, J., G.M. Laslett, and A.B. McBratney. 2000. Calibrating an electromagnetic induction instrument to measure salinity in soil under irrigated cotton. Soil Sci. Soc. Am. J. 64:1009–1017. doi:10.2136/sssaj2000.6431009x

U.S.D.A. 1954. Diagnosis and improvement of saline and alkaline soils, U.S.D.A. Agricultural Handbook 60, edited by L.A. Richards, U.S. Govt. Print. Off., Washington, D.C.

Vachaud, G.A., A. Passerat de Silans, P. Balabanis, and M. Vauclin. 1985. Temporal stability of spatially measured soil water probability density function. Soil Sci. Soc. Am. J. 49:822–828. doi: 10.2136/sssaj1985.03615995004900040006x

Vanderlinden K., H. Vereecken, H. Hardelauf, M. Herbst, G. Martinez, M.H. Cosh, and Y.A. Pachepsky. 2012. Temporal Stability of Soil Water Contents: A Review of Data and Analyses. Vadose Zone Journal 11. DOI: Doi 10.2136/Vzj2011.0178.

Vereecken H., J.A. Huisman, Y. Pachepsky, C. Montzka, J. van der Kruk, H. Bogena, L. Weihermuller, M. Herbst, G. Martinez, and J. Vanderborght. 2014. On the spatio-temporal dynamics of soil moisture at the field scale. Journal of Hydrology 516:76-96. doi:10.1016/j.jhydrol.2013.11.061.

Werban U., H. Bartholomeus, P. Dietrich, G. Grandjean, and S. Zacharias. 2013. Digital Soil Mapping: Approaches to Integrate Sensing Techniques to the Prediction of Key Soil Properties. Vadose Zone Journal 12. doi:10.2136/vzj2013.10.0178.

Zacharias S., H. Bogena, L. Samaniego, M. Mauder, R. Fuß, T. Pütz, M. Frenzel, M. Schwank, C. Baessler, K. Butterbach-Bahl, O. Bens, E. Borg, A. Brauer, P. Dietrich, I. Hajnsek, G. Helle, R. Kiese, H. Kunstmann, S. Klotz, J.C. Munch, H. Papen, E. Priesack, H.P. Schmid, R. Steinbrecher, U. Rosenbaum, G. Teutsch, H. Vereecken. 2011. A network of terrestrial environmental observatories in Germany. Vadose Zone J 10:955-973.

Zhu Q., H. Lin, J. Doolittle. 2010. Repeated Electromagnetic Induction Surveys for Determining Subsurface Hydrologic Dynamics in an Agricultural Landscape. Soil Science Society of America Journal 74:1750-1762. doi:10.2136/sssaj2010.0055.